2019A1219 BL40B2

Towards Corneal Structure Mapping in the Living Eye Using a Combined X-ray Scattering, Biomedical Imaging and Machine Learning Approach

Craig Boote[a], Michael J. A. Girard[b], Alexandre H. Thiery[c], Noboru Ohta[d]

[a]School of Optometry & Vision Sciences, Cardiff University
[b]Opthalmic Engineering & Innovation Laboratory, Singapore Eye Research Institute
[c]Institute for Mathematical Science, National University of Singapore
[d]Japan Synchrotron Radiation Research Institute

Abstract

Corneal blindness is a leading cause of vision loss worldwide. Corneal curvature and transparency depend on the cornea's unique collagen fibril architecture and, while much progress has been made in mapping collagen structure in cadaveric corneas, there is currently no way of imaging collagen fibril organization in the living eye. Our ultimate goal is to develop new artificial intelligence (AI)-assisted bioimaging technology to map collagen structure in live patient corneas. Here we present results from SPring-8 beamline BL40B2 in the form of wide-angle X-ray scattering (WAXS) maps of corneal structure from ex-vivo porcine eyes, which were previously scanned via optical coherence tomography (OCT), and will be used as a platform to train machine learning algorithms to "read" the equivalent in-vivo data from OCT images obtained from human patients.

Keywords: Cornea, Collagen, X-ray Scattering, Optical Coherence Tomography, Machine Learning

Background and Purpose

The human cornea is composed of around 200 stacked layers ("lamellae"), which lie parallel to the corneal surface [1]. Each lamella contains uniformly narrow, regularly spaced collagen fibrils embedded in a hydrated extrafibrillar matrix. Fibrils within a lamella lie parallel but subtend large angles with adjacent lamellae [2]. As collagen is the major load-bearer, fibril organization has a major influence on corneal biomechanical behaviour [3], and hence the cornea's ability to maintain curvature under intraocular pressure (IOP), eye-movements and external physical trauma. We have developed the use of synchrotron X-ray scattering to map the collagen fibril organization of the ex-vivo cornea (reviewed [4]). This work has shown that the cornea is a highly anisotropic and regionally variable tissue [5], which shows specific structural changes in response to corneal disease [6-8] and surgery [9-11]. However, there exists no similarly effective and validated method which can be applied safely in the living eye. The current project aims to address this shortfall by leveraging recent improvements in biomedical image processing and combining them with machine learning algorithms trained using ex-vivo X-ray scattering data in a porcine model. In brief, the experimental approach has three overarching stages:

Stage 1 - Optical Coherence Tomography (OCT) Imaging (Singapore Eye Research Institute)

Corneas in intact, enucleated eyeballs from pigs are imaged using a Spectralis OCT device. 3D image stacks are post-processed using corneal adaptive compensation developed by the authors to enhance corneal OCT images to improve tissue contrast, remove image artefacts, and increase visibility of corneal lamellae [12].

Stage 2 – X-ray Scattering (SPring-8 BL40B2)

Following OCT imaging, porcine corneas are fixed in their in-situ curvature using paraformaldehyde, dissected (retaining 3mm of scleral rim) and shipped to SPring-8 BL40B2 for X-ray analysis. The experimental details are described in detail in the Experimental Summary section below and are based on beamline set-ups we developed previously at SPring-8 [13-15] and other synchrotrons [5,11,16]. Corneal collagen fibril organization parameters from the X-ray maps are correlated with OCT image volumes using machine learning algorithms in Stage 3.

Stage 3 - Machine Learning (National University of Singapore)

The training datasets obtained in Stages 1 and 2 are comprised of pairs of ex-vivo pig corneal data volumes, each consisting of a high-resolution, enhanced 3D OCT volume and corresponding 2D WAXS maps (the latter

representing a depth-integrated 3D volume). After a standard alignment of the depth-integrated 3D OCT volumes with their corresponding 2D collagen orientation maps, a convolutional network is fitted to obtain a machine learning algorithm capable of interpreting the collagen orientation map from any ex-vivo corneal OCT volume, and ultimately in any live patient eye. Similar 3D convolutional networks have been developed by the authors for obtaining segmented tissue geometry maps of OCT volumes in other eye tissues [17], however the current proposal is the first to aim to extend the technology to image tissue microstructure.

Experimental Summary

BL40B2 was used in a custom fibre wide-angle X-ray scattering (WAXS) set-up adapted primarily from previously published work at the Daresbury and Diamond UK synchrotrons (reviewed [4]). A schematic of the basic beamline set-up is shown in Fig. 1A. A combination of a 0.1nm monochromatic x-ray beam and a 2D area detector (Dectris Pilatus 3S 2M) positioned 318 mm behind the specimen was employed to allow full 360º angular resolution of the equatorial reflection from the regular ~1.5nm lateral spacing of tropocollagen molecules within the type I corneal fibrils [18] (Fig. 1B).

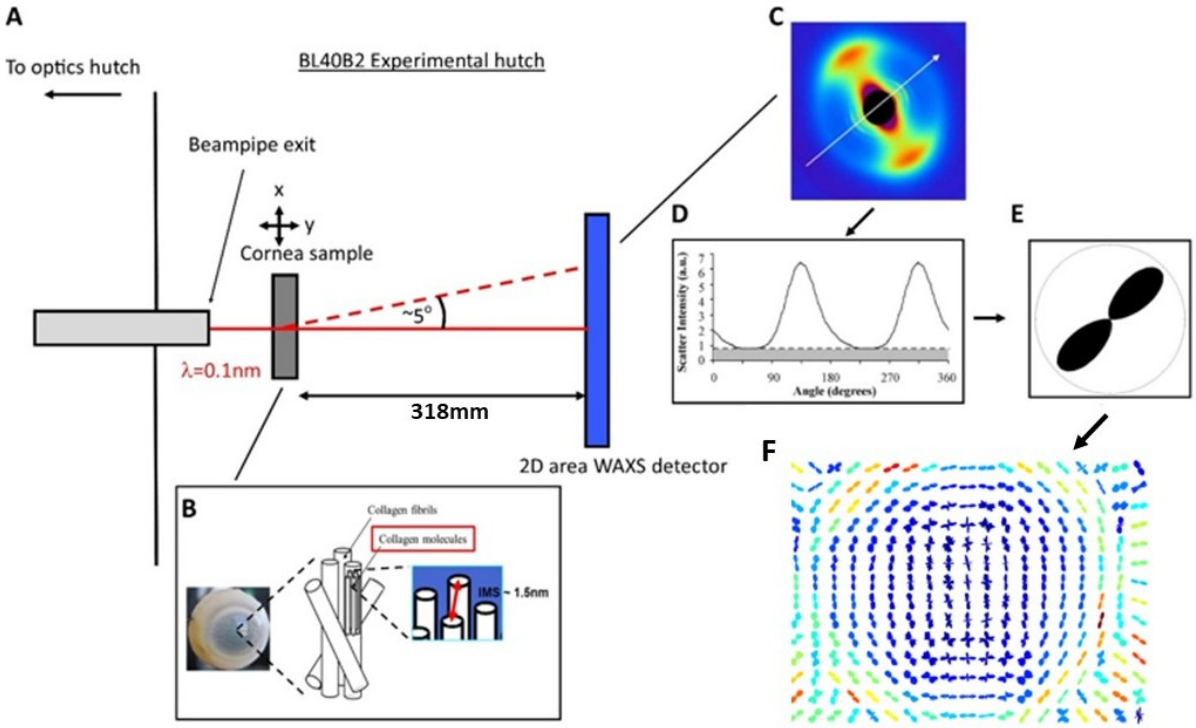

Fig. 1. Use of BL40B2 to map corneal collagen fibril structure. **A)** Beamline set up in WAXS fibre mode. **B)** Regular 1.5nm collagen intermolecular spacing is used to derive the WAXS signal. **C)** Lobed equatorial WAXS pattern from collagen oriented along the direction of the white arrow. **D)** Azimuthal scatter intensity distribution. **E)** Polar vector plot of collagen orientation. **F)** Assimilation of individual data point plots into orientation map of porcine cornea. Warmer colours indicate higher collagen anisotropy.

Using the molecular WAXS signal for corneal collagen mapping has two major advantages over small-angle X-ray scattering (SAXS – which in contrast derives from the fibrils themselves): 1) The WAXS signal is far more stable under variations in tissue hydration and the presence of other collagen-bound molecules (e.g. proteoglycans), and 2) The WAXS signal (Fig 1C) is a single, pure equatorial peak - as opposed to being a complex combination of equatorial and meridional scatter components (as in SAXS) [19], which can often be difficult to uncouple. Corneas with scleral rim (pre-fixed to retain natural tissue curvature) were film-wrapped to minimize tissue dehydration and mounted intact inside Perspex cells. The beamline motor stages were used to translate the specimen in x and y between X-ray exposures to map the tissue at spatial intervals of 1mm in each direction. The beam-size at the specimen measured 0.3 mm x 0.3 mm and ensured bulk coverage of the cornea without re-exposing neighbouring sampling sites. The X-ray exposure time per data point was 1s and the approximate X-ray transmission pathlength was 1-1.5 mm. A total of 15 pig corneas were scanned in their natural curvature, with the X-ray beam directed normal to the corneal surface at the apex (i.e. replicating the set-up of the complimentary OCT experiments). Powdered $CaCO_3$ was used to precisely determine the WAXS pattern centre prior to orientation analysis. We have computational protocols

in place to extract orientation information from the WAXS patterns, and these are described in detail in the literature [4]. In brief, a bespoke 2D background function isolated the collagen WAXS signal by removing scatter from the specimen cell and non-collagen components of the corneal tissue. The WAXS peak was then radially integrated and extracted into 720 azimuth angle bins to obtain the precursory fibril orientation distribution (Fig. 1D). A deconvolution correction was applied to the precursory orientation distribution to account for the 15° microfibrillar tilt of the tropocollagen molecules with respect to the fibrillar long axis [20], and then the corrected fibril orientation distribution was expressed in polar vector coordinates (Fig. 1E). Individual polar vector plots from each sampling point were assimilated into maps to visualize the variation in collagen fibril orientation across each pig cornea (Fig. 1F). The corrected orientation distribution (resolved into relative collagen fibril number per half degree of azimuth angle within the corneal plane) of each pig cornea was then compared with corresponding depth-integrated, ex-vivo 3D OCT volumes to form the "training step" of a machine learning algorithm, which will subsequently be adapted to extract collagen maps from in-vivo OCT image volumes of living corneas.

Results and Discussion

15 porcine corneas were scanned using WAXS at an x-y sampling resolution of 0.5 mm. Maps of preferential fibril orientation, total collagen scatter and degree of collagen anisotropy at each sampled point were obtained from the analysis (see Fig 2). The results showed that the pig cornea is anisotropic and characterized by weakly orthogonally oriented collagen in the central (pre-pupil) region (Fig 2B), while the fibrils become increasingly circumferentially aligned on approaching the limbus (junction of the cornea and sclera - see Fig 2A) – with maximal anisotropy observed in the oblique limbal regions (Figs 2B and 2D).

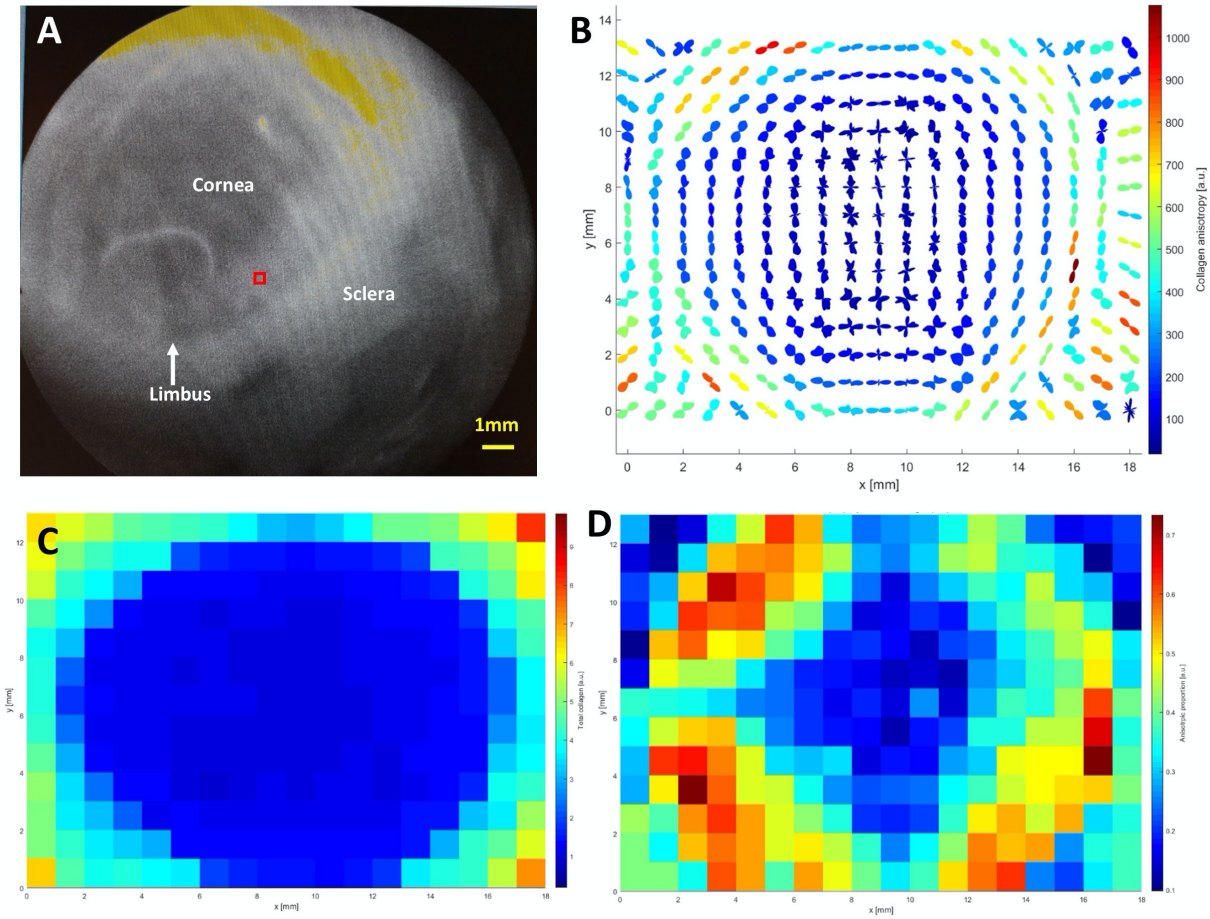

Fig. 2. WAXS results from porcine cornea, obtained using SPring-8 beamline BL40B2. **A)** Beamline camera image of mounted porcine anterior eye chamber with cornea, sclera and limbus (corneo-scleral junction) labelled. The red square marks the area of tissue exposed with X-rays at each data point. **B)** Vector map of collagen fibril orientations across specimen at 1mm x 1mm spatial resolution. Vector plot shapes indicate dominant fibril directions (orthogonal in the corneal centre, circumferential in the corneal periphery/limbus and radial in the sclera), while colours denote anisotropy. **C)** Contour map of total collagen scatter. Increased scatter in the limbus and sclera reflects tissue thickening from cornea to limbus and increased collagen fibril size/density in the sclera. **D)** Contour map of collagen anisotropy, showing higher levels of collagen reinforcement in the oblique regions of the peripheral cornea and limbus.

Biomechanically, reinforcement of the limbal region with circumferential collagen is consistent with requirements for maintenance of corneal shape in a region where changes in curvature and material properties between cornea and sclera are predicted to result in locally increased tissue stress [7]. The sclera (white tissue of the eyeball coat) was characterized by strongly radially aligned collagen (Fig 2B), likely associated with directions of force transduction from the extraocular muscles [21]. Notably, the structural features seen in the pig cornea closely mimic those in the human eye [5], marking the pig as an appropriate starting point for protocol development.

The WAXS results presented here will be used to extract corresponding data from enhanced OCT images via machine learning. Once validated in the porcine model, we will extend the technology to human corneas (initially in cadaveric eye globes and then in live patients). This can potentially have significant future impact in global healthcare, with immediate ophthalmic applications in keratoconus screening [6] and post-surgical monitoring of corneal transplant patients [10,11]. Further adaption of the method could possibly enable imaging of collagen structure at the back of the eye, opening up possible applications in glaucoma and myopia clinics [22,23], and more widely in other systemic connective tissue diseases.

Challenges

The accurate registration of 2D WAXS data with 3D OCT image stacks is key to success of the project and represents a major challenge. While pre-fixation of porcine eyeballs under simulated eye pressure minimizes corneal curvature changes upon dissection for WAXS experiments, a more optimal approach would be to carry out both OCT and WAXS in intact eyeballs – possibly through the development of back-scattered WAXS approaches. Moreover, bridging the large resolution gap between collagen structure levels probed by WAXS (nm range) and OCT (μm range) will require advanced AI algorithms with extremely high sensitivity and specificity. Prominent collagen anisotropic features within the limbus and sclera will serve as focal points for feature recognition, however more subtle features in the central cornea will be far more difficult to capture and recognize. While this issue has been partially addressed already through the development of adaptive corneal compensation technologies to allow clearer visualization of corneal lamellae in OCT images [12], further optimization is required to move towards possible clinical translation.

References

[1] D. Maurice, *J. Physiol.*, **136**, 263 (1957).
[2] Y. Komai and T. Ushiki, *Invest. Ophthalmol. Vis. Sci.*, **32**, 2244 (1991).
[3] C. Boote *et al*., *J. Struct. Biol.*, **149**, 1 (2005).
[4] K. Meek and C. Boote, *Prog. Retin. Eye Res.*, **28**, 369 (2009).
[5] C. Boote *et al*., *Invest. Ophthalmol. Vis. Sci.*, **47**, 901 (2006).
[6] S. Hayes *et al*., *Exp. Eye Res.*, **84**, 423 (2006).
[7] C. Boote *et al*., *J. Struct. Biol.*, **166**, 195 (2009).
[8] S. Morgan *et al*., *Biophys. J.*, **104**, 2586 (2013).
[9] C. Kamma-Lorger *et al.*, *Mol. Vis.*, **15**, 378 (2009).
[10] S. Hayes *et al*., *Eye*, **4**, 728 (2010).
[11] C. Boote *et al*., *PLoS One*, **8**, e68166 (2013).
[12] M. Girard *et al*., *Transl. Vis. Sci. Technol.*, **4**(3), 3 (2015).
[13] A. Quantock *et al*., *J. Appl. Crystallogr.*, **40**, S335 (2007).
[14] S. Hayes *et al*., *PLoS One*, **8**, e52860 (2013).
[15] B. Palka *et al*., *Curr. Eye Res.*, **35**, 580 (2010).
[16] C. Boote *et al*., *Biophys. J.*, **101**, 33 (2011).
[17] S. Devalla *et al*., *Invest. Ophthalmol. Vis. Sci.*, **59**, 63 (2018).
[18] K. Meek and C. Boote, *Exp. Eye Res.*, **78**, 503 (2004).
[19] K. Meek and A. Quantock, *Prog. Retin. Eye Res.*, **20**, 95 (2001).
[20] S. Yamamoto *et al*., *Arch. Histol. Cytol.*, **63**, 127 (2000).
[21] C. Boote *et al*., *Prog. Ret. Eye Res.*, **74**, 100773 (2020).
[22] I. Campbell *et al*., *J. Biomech. Eng.*, **136**, 021005 (2014).
[23] P. Markov *et al*., *Mol. Vis.*, **24**, 818 (2018).

(Received: September 28, 2022; Accepted: October 11, 2022; Published: February 28, 2023)